ACS Photonics

Article

Cite This: ACS Photonics 2019, 6, 501−509

pubs.acs.org/journal/apchd5

Hybrid Metasurface-Based Mid-Infrared Biosensor for Simultaneous Quantification and Identification of Monolayer Protein

Zhaoyi Li,*[,†,‡,§] Yibo Zhu,[†,∥,⊥] Yufeng Hao,[∥] Ming Gao, Ming Lu,[▽] Aaron Stein,[▽] Ah-Hyung Alissa Park,[#] James C. Hone,[∥] Qiao Lin,*[,∥] and Nanfang Yu*[,‡]

[‡]Department of Applied Physics and Applied Mathematics, Columbia University, New York, New York 10027, United States

[§]Harvard John A. Paulson School of Engineering and Applied Sciences, Harvard University, Cambridge, Massachusetts 02138, United States

[∥]Department of Mechanical Engineering, Columbia University, New York, New York 10027, United States

[⊥]Coherent AI LLC, Redwood City, California 94065, United States

[#]Department of Earth and Environmental Engineering, Columbia University, New York, New York 10027, United States

[▽]Center for Functional Nanomaterials, Brookhaven National Laboratory, Upton, New York 11973, United States

Supporting Information

ABSTRACT: Metasurfaces emerge as a promising photonic platform for biosensing because they offer strong optical confinement and tunable optical resonances. Here, we show that metasurface-based biosensors consisting of gold nanoantenna arrays loaded with graphene and working in the mid-infrared (mid-IR) spectral range can achieve simultaneous high-sensitivity and high-specificity detection of biomolecules. Strong light−molecule interactions in deeply subwavelength optical spots created by the biosensors allow us to determine the concentration of protein molecules via spectral shifts of the metasurface resonance. A combination of passive and active tuning of the metasurface sensors allows us to spectrally overlap the metasurface resonance and the protein vibrational modes, so that protein molecules can be identified via their characteristic mid-IR "fingerprints". The high sensitivity and specificity of the metasurface sensors enable us to determine the secondary structure of protein immunoglobulin (IgG) molecules 4 orders of magnitude more sensitive than attenuated total reflection Fourier transform infrared spectroscopy.

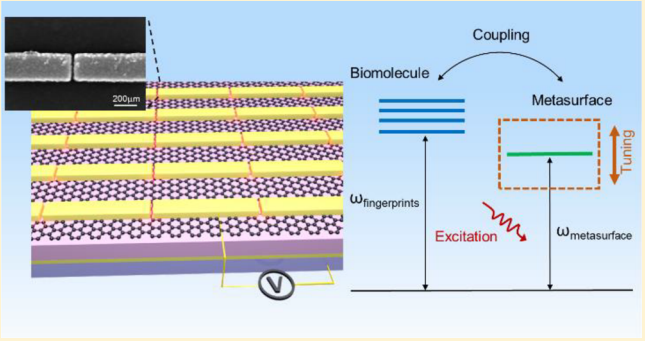

KEYWORDS: *hybrid metasurface, graphene, mid-infrared biosensor, tunable fingerprinting, secondary structure*

Understanding the biomolecules interaction and probing their molecular structures are critical to address challenges in both fundamental biological studies and practical biomedical applications. Biosensing technologies based on different principles have been developed, such as electrochemical reactions,[1] surface plasmon resonances,[2,3] and field-effect transistors,[4,5] but most of them only allow for sensitive quantification, but cannot provide structural information on analytes. Although selective binding between receptors and target molecules can be employed to improve the sensor specificity, it remains difficult to confirm the species adsorbed on the sensor surface due to the lack of structural details of these species. This, on the other hand, makes it challenging to interpret the sensor output in practical measurements, which can be induced by the binding of target molecules or nonspecific adsorption and variation in environmental conditions such as temperature and ionic strength.

To improve the sensing specificity and to confidently determine the composition of analytes, the information on molecular structures is needed. Such information usually can be acquired using spectroscopic techniques, for example, Raman spectroscopy,[6,7] X-ray crystallography,[8] nuclear magnetic resonance,[9] circular dichroism spectroscopy,[10] and Fourier transform infrared spectroscopy.[11−13] Compared to electrical or electrochemical sensing methods, the spectroscopy-based approach provides a unique opportunity to achieve both quantitative measurement and fingerprinting of biomolecules. Unfortunately, it is still difficult to realize these two functionalities in one single device, which at least requires complicated analytical models, time-consuming mapping,[14] or complementary acquisition of optical spectra using different instruments.[15]

The fact that there has been thus far limited success in realizing simultaneous quantification and identification of molecules is due to the needs of two conflicting features of optical devices: On one hand, a narrow spectral line width with

Received: October 22, 2018
Published: January 23, 2019

DOI: 10.1021/acsphotonics.8b01470
ACS Photonics 2019, 6, 501−509

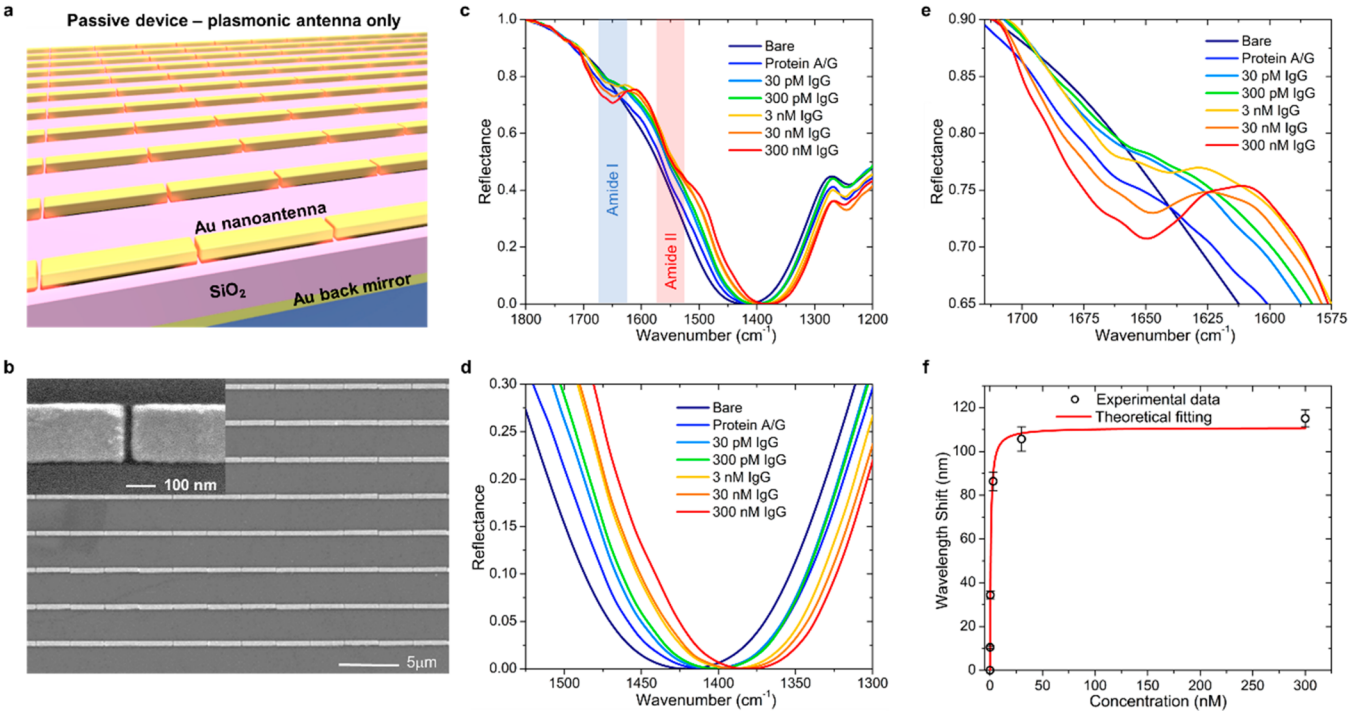

Figure 1. Performance of passive metasurface sensors as a function of protein concentration. (a) Schematic of a passive metasurface sensor, which consists of gold nanorod antennas, a 400 nm SiO_2 spacer, and a gold back mirror. The gaps between adjacent nanoantennas have a width of 30 nm. (b) SEM image of a metasurface sensor, showing uniform nanoantenna geometry and gap sizes. Inset: zoom-in view of one antenna gap. (c) Measured reflectance spectra of the device after physisorption of a monolayer protein A/G and subsequent binding with antibody IgG molecules with different concentrations. The Amide I and Amide II bands are shadowed in blue and red, respectively. (d) Zoom-in view of (c), showing the red shifts of the metasurface resonance as a result of an increase of the local optical refractive index caused by protein immobilization. (e) Zoom-in view of (c), showing that the absorption dips corresponding to the Amide I band increase in magnitude as the device was incubated in protein IgG with increasing concentrations. (f) Measured wavelength shifts of the metasurface resonance as a function of protein IgG concentration, and fitting to the experimental data using the Langmuir adsorption isotherm model.

high quality factor (Q factor) is desirable for sensing the concentation of biomolecules. For most optical sensors, binding of molecules causes changes in the local effective refractive index of optical resonators, resulting in a shift of the resonant wavelength. A narrower resonant line width with higher Q factor allows for the observation of a smaller detectable spectral shift and thus higher detection sensitivity.[16−19] On the other hand, for molecular fingerprinting, such high Q-factor optical resonances may not be desirable as there would be significant mismatch between the sharp optical resonances and the spectral fingerprints located at different frequencies.[20,21] To meet both requirements, one needs not only to engineer the quality factor of resonance, but also to precisely control the resonance frequency for biosensing.

Metasurfaces, two-dimensional assemblies of subwavelength optical antennas,[22−24] have emerged as a new photonic platform for biosensing.[12,16,25,26] Resonant excitation of optical antennas concentrates optical energy into volumes substantially smaller than diffraction-limited optical spots,[27,28] which are suitable for detecting small quantities of biomolecules. It is particularly interesting that, in the mid-infrared (mid-IR) spectral region, the resonant responses of metasurfaces can be tuned to overlap with and enhance the spectral fingerprints of a vast variety of biological building blocks.[25] Recently,the active tuning of graphene plasmon resonance has been exploited in mid-IR biosensor to selectively probe the fingerprints of protein at different frequencies.[20,21] It remains a challenge to simultaneously achieve high sensitivity quantification and high specificity identification of biomolecules in a single photonic platform, which requires engineering of the resonance quality factor and precise tuning of the resonance frequency at the same time.

Here, we present metasurface-based compact mid-IR biosensors that enable simultaneous quantification and fingerprinting of protein molecules with high sensitivity and specificity. The metasurfaces used in this work, consisting of gold nanoantennas separated by nanometer gaps and loaded with graphene, support an optical resonance with an intermediate Q-factor of ∼10 in the mid-IR region. The optical resonance can be adjusted by choosing proper antenna lengths and further fine-tuned by controlling the carrier doping of graphene via a bias voltage to more closely overlap the biomolecular fingerprints. Using such metasurface-based biosensors, we simultaneously analyzed the small quantity of protein specifically binding to the receptor-decorated sensor surface through the resonance frequency shifts, and identified the protein species via enhanced fingerprinting. We also systemically studied the near-field optical enhancement effects using both metallic metasurface and tunable graphene-metallic hybrid metasurface. These results further allowed us to quantitatively determine the secondary structures of proteins with unprecedented sensitivity and accuracy by considering the shift of the vibrational resonance induced by the coupling of the molecules phonon resonance and the metasurface plasmon resonance.

The metasurface biosensors consist of array of gold nanorod antennas separated from a gold back mirror by a 400 nm SiO_2 spacer layer (Figure 1a). The gap between adjacent antennas is

DOI: 10.1021/acsphotonics.8b01470
ACS Photonics 2019, 6, 501−509

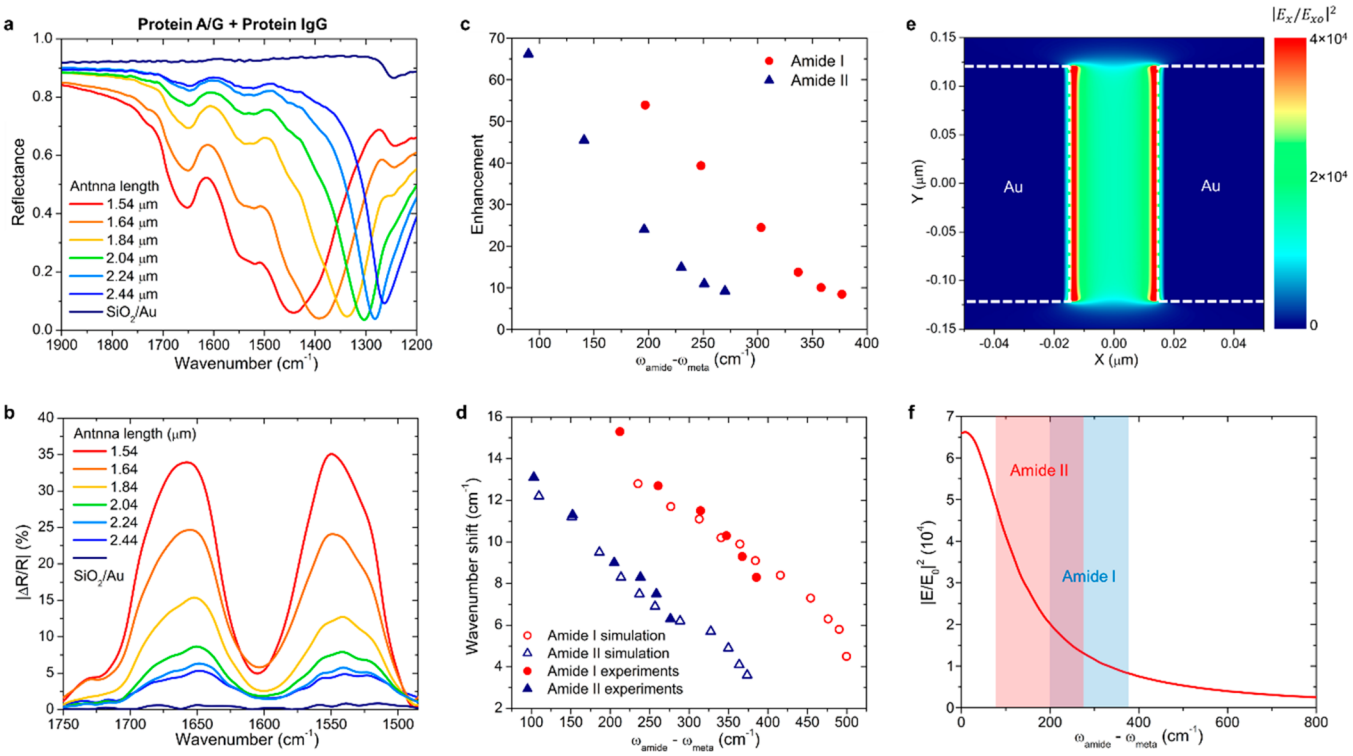

Figure 2. Performance of passive metasurface sensors with different nanoantenna lengths. (a) Measured reflectance spectra of devices with different nanoantenna lengths after immobilization of a monolayer protein A/G and a monolayer antibody IgG. The lengths of nanoantennas range from L = 1.54 to 2.44 μm. The magnitude of the Amide I and Amide II fingperprints increases as the frequency difference between the amide bands and the metasurface resonance decreases. In comparison, the Amide I and II bands measured from the protein double layer immobilized on a bare SiO_2/Au substrate are very weak. (b) Measured relative absorptance spectra of the amide bands extracted from (a). (c) Measured enhancement of relative absorptance of the amide bands in metasurface sensors compared to a control device consisting of a SiO_2/Au substrate. (d) Comparison between measured and simulated spectral shifts of the amide bands, extracted from a and d, as a function of $\omega_{amide} - \omega_{meta}$. (e) Simulated near-field distributions of light intensity normalized to the intensity of the incident light, that is, $|E_x/E_{x0}|^2$ around one antenna gap at ω = 1460 cm^{-1}. Additional simulation results (XZ cross section) are provided in Supporting Information, Section IV. (f) Simulated light intensity enhancement averaged over the interface between SiO_2 and air inside the nanoantennas gap as a function of $\omega_{amide} - \omega_{meta}$. Shadowed regions correspond to the Amide I band and the Amide II band.

30 nm, which is consistent through the entire metasurface sensor (Figure 1b). A beam of incident infrared light polarized along the antenna rods excites strong plasmonic resonance in the antennas. The near-field coupling between the nanorod antennas and their dipolar images in the back mirror forms a quadrupole, which suppresses radiative losses and increases the Q-factor of the plasmonic resonance.[29,30] Furthermore, the plasmonic mode couples strongly with the phonon resonance in the SiO_2 spacer layer, creating two hybrid plasmon-phonon modes, which lead to two sharp dips in the device reflectance spectra (Supporting Information, Section V). The spectral dip closer to the mid-IR fingerprints of protein molecules is utilized for biosensing with a Q-factor of ~10. The collective effects of small and uniform antenna gaps, the coupling between the antennas and the back mirror, and the plasmon-phonon interactions result in a local electric field intensity 4 orders of magnitude stronger than the incident light according to full-wave simulations (see below), which enables us to achieve strong enhancement of the mid-IR molecular fingerprints that overlap the plasmonic resonance in optical frequency.

In this study, human antibody immunoglobulin G (IgG) was used as a representative target protein. In the quantitative measurement of the IgG concentration, recombination protein A/G was employed as a high-affinity receptor of IgG (Supporting Information, Section II).[12,16,19,25,26,31] Prepration and process of the protein samples for biosensing followed established protocal (see details in the Methods section). Briefly, monolayer A/G was first formed by physisorption, and IgG solutions with different concentrations were drop-coated on the sensor and incubated for 1 h to allow for the binding to reach equilibrium.[20,31] Figure 1c shows that as the concentration of IgG increased, the metasurface resonance red-shifted (i.e., moved toward smaller wavenumbers; Figure 1d) due to the increase in the optical refractive indices in the vicinity of gold nanorod antennas (mainly from gaps as shown in Supporting Information, IV) upon binding of IgG to the protein A/G. At the same time, there were two spectral dips, which were respectively located in the ranges of 1620−1680 cm^{-1} (ω_I) and 1510−1580 cm^{-1} (ω_{II}), showing monotonical inrease in intensity with the concentration of IgG (Figure 1c,e). These two absorption bands at ω_I and ω_{II} should be respectively assigned to the Amide I and Amide II vibrational modes of protein molecules.[11] Compared with most plasmonic biosensors that quantify analytes soly relying on the shift of the plasmonic resonance, our plasmonic sensor provides additional fingerprints information. The correlation between the redshifts of the optical resonance and the intensity of amide fingerprints serves as strong evidence that the redshifts of the plasmonic resonance peak indeed arose from the binding between the

DOI: 10.1021/acsphotonics.8b01470
ACS Photonics 2019, 6, 501−509

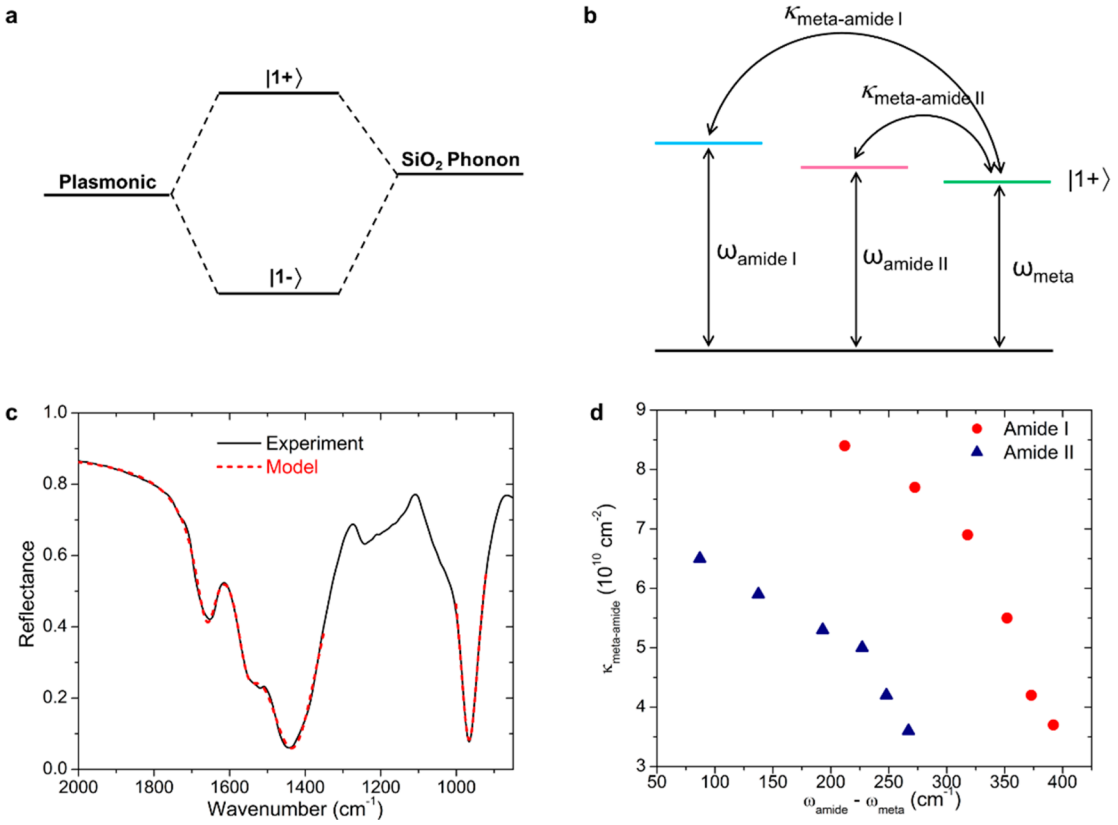

Figure 3. Coupled oscillator model. (a) Coupling between the plasmonic mode in the nanoantennas and the phonon resonance mode in the SiO_2 spacer layer creates two hybrid plasmon-phonon modes. One of the plasmon-phonon modes, labeled as $|1+\rangle$, with a higher frequency and spectrally closer to the mid-IR fingerprints of protein molecules is utilized for biosensing. (b) Diagram showing the coupling between the plasmon-phonon mode $|1+\rangle$ and the amide modes via coupling coefficients $\kappa_{\text{meta-amide I(II)}}$. (c) Black curve: Measured reflectance spectrum of a metasurface sensor after immobilization of a monolayer protein A/G and a monolayer antibody IgG. The length of nanoantennas is $L = 1.54$ μm. Red curve: Fitting to the measured spectrum (excluding the phonon resonance of SiO_2 around 1000−1350 cm^{-1}) using the coupled oscillator model. (d) Extracted coupling coefficients $\kappa_{\text{meta-amide}}$ from the fitting, showing increased coupling strength as the frequency differences between the metasurface resonance and the amide vibrational phonon resonances decreases.

sensor and the target protein, instead of from nonspecific adsorption or fluctuation in environmental condictions such as temperature. The lowest IgG concentration that can be confidently resolved using our sensor was 30 pM, comparable to the state-of-the-art values reported.[19,31] The shifts of the metasurface resonance as a function of the IgG concentration can be well fitted by the Langmuir adsorption isotherm model (Figure 1f),[19,32] delivering a dissociation constant of $K_d = 0.71$ nM for the interaction between human antibody IgG and protein A/G.

In the following sections, we present a more quantitative study of the enhancement effects, which later not only leads us to explore methods to more efficiently enhance the fingerprints of interest, but also allows us to perform a finer analysis of the protein structures using the enhanced fingerprints. First, we tuned the metasurface resonance by varying the length of nanoantennas to enhance the amide bands of a protein bilayer consisting of monolayer IgG captured by monolayer protein A/G on the sensor surface. When the antenna length L was decreased from 2.44 to 1.54 μm, the metasurface resonance blue-shifted from 1263 to 1443 cm^{-1}, closer to the amide vibrational modes. Consequently, the amide spectral dips increased in magnitude significantly (Figure 2a), in excellent agreement with full-wave simulations (Supporting Information, V).

We then compared the relative absorptance, defined as $|\Delta R/R| = |(R - R_{IgG})/R|$, of the Amide I and Amide II bands after enhancement on six independent metasurfaces with different antenna lengths. Here R_{IgG} represents the reflectance spectra of devices with a monolayer of IgG, and R represents polynomial fits to the experimental spectra, excluding the amide bands (i.e., ω_I = 1620−1680 cm^{-1} and ω_{II} = 1510−1580 cm^{-1}) (Supporting Information, Section VI). The relative absorptance peak value of Amide I in the differential spectra increased from 5.3% to 34.0% as the spectral difference between the metasurface resonance and the Amide I vibrational frequency, $\Delta\omega = |\omega_{meta} - \omega_{amideI}|$, decreased from 377 to 197 cm^{-1} (Figure 2b). Similarly, the relative absorptance peak value of Amide II increased from 4.8% to 35.1% as $\Delta\omega = |\omega_{meta} - \omega_{amideII}|$ decreased from 270 to 90 cm^{-1}. In comparison, our experiments show that the relative absorptance peak value of the Amide I and II bands was only 0.63% and 0.69%, respectively, when protein A/G and antibody IgG monolayers were incubated on a control device without nanoantennas (i.e., only 400 nm SiO_2 on a gold substrate; spectrum labeled as "SiO_2−Au" in Figure 2b). The large enhancement of the amide bands (Figure 2c) is owing to strong light−matter interactions inside the antenna gaps. Full-wave simulations show that optical power of the incident light is strongly localized inside the gaps (Figure 2e, Supporting Information, IV). The light intensity enhancement at the amide bands is typically 1×10^4−

DOI: 10.1021/acsphotonics.8b01470
ACS Photonics 2019, 6, 501−509

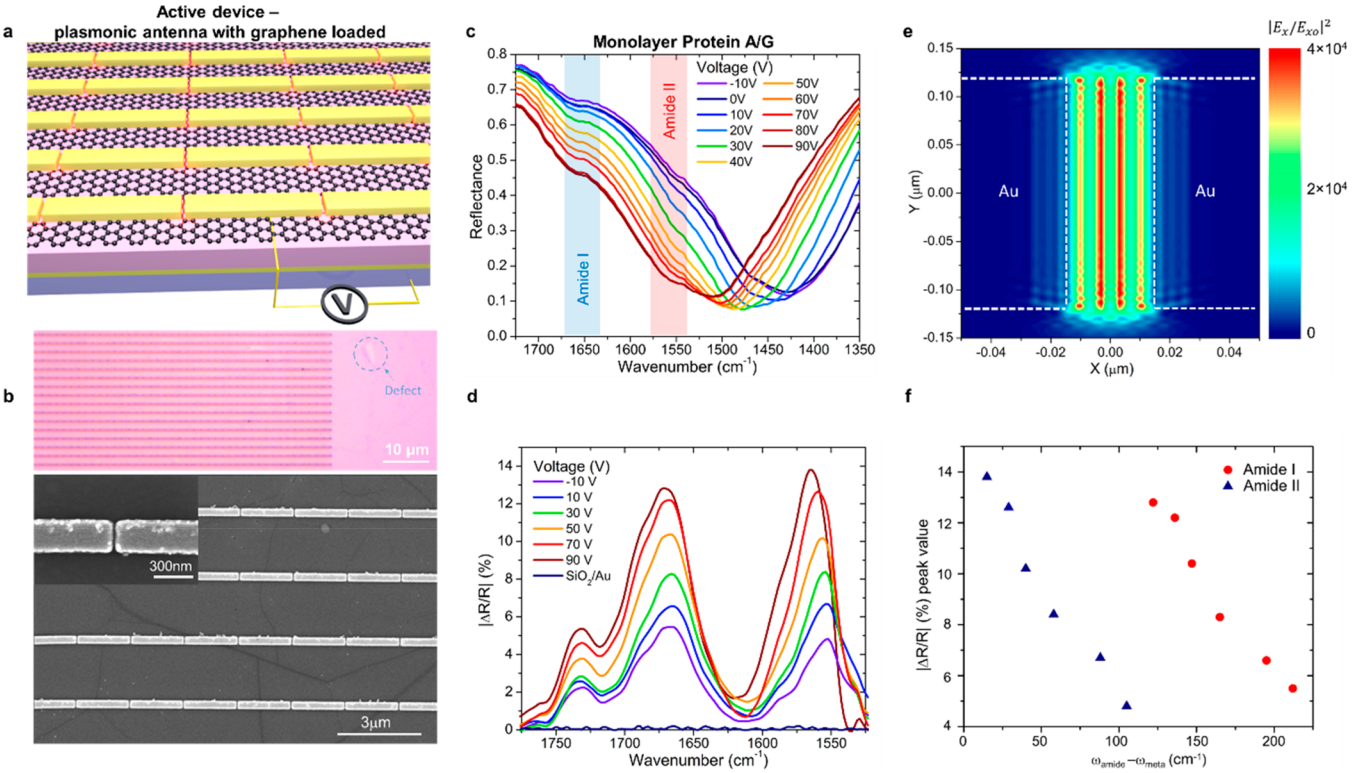

Figure 4. Active metasurface sensors for protein fingerprinting. (a) Schematic of an active metasurface sensor. The Fermi level of graphene can be tuned via a gate voltage applied between an electrical contact on graphene and the Pt back mirror. (b) Optical image and SEM image of one device showing nanoantennas patterned on an SiO_2/Pt substrate coated with a single-layer graphene. Inset: Zoom-in view of one antenna gap showing that the gap width is ~30 nm. (c) Measured reflectance spectra of an active device incubated with a monolayer protein A/G and measured at different gate voltages. The Amide I and II bands are shaded in blue and red, respectively. (d) Relative absorptance spectra of the amide bands at different gate voltages extracted from (c). (e) Simulated near-field distributions of light intensity normalized to the intensity of the incident light, i.e., $|E_x/E_{x0}|^2$, around one antenna gap at ω = 1645 cm^{-1}. (f) The peak value of relative absorptance of amide bands as a function of frequency differences between the metasurface resonance and the amide bands vibrational phonon resonances.

5×10^4 averaged over the gap area (Figure 2f). We observed blueshifts of the peak position of the amide bands as the difference between the metasurface resonant frequency and the amide bands frequencies decreases (Figure 2d). This phenomenon was verified in full-wave simulations (Supporting Information, VII) and has been observed in strongly coupled systems consisting of plasmons and molecular vibrations.[33,34]

To better understand the interactions between light and protein molecules mediated by the metasurface, we developed a coupled oscillator model (Figure 3a,b) and fitted experimental data using this model (Supporting Information, Section VIII). Four oscillators are considered in our model: plasmonic resonance of gold nanoantennas, phonon resonance of the SiO_2 spacer, and Amide I and II vibrational modes. This model predicts that a smaller spectral separation between the amide modes and the metasurface plasmon−phonon mode, $\Delta\omega = |\omega_{meta} - \omega_{amide}|$, and larger coupling coefficient, $\kappa_{meta\text{-}amide}$, between the two lead to larger susceptibility of the amide oscillators. By fitting measured spectra using the coupled oscillator model (antenna length L = 1.54 μm as an example in Figure 3c), we extracted $\kappa_{meta\text{-}amide}$ from the six metasurface sensors with different antenna lengths (Figure S8), and found that $\kappa_{meta\text{-}amide}$ for both amide bands increased as the frequency difference $\Delta\omega = |\omega_{meta} - \omega_{amide}|$ decreased (Figure 3d). Furthermore, at the same $\Delta\omega$, $\kappa_{meta\text{-}amide}$ for Amide I was larger than that of Amide II, indicating that the C═O stretching vibrations associated with the Amide I band are more easily excited by optical near-fields than the N−H bending and C−N stretching vibrations associated with the Amide II band.

We note that although the fingerprints can be effectively enhanced on the passive metasurface, accurate control of the enhancement effect at a specific spectral range of interest can be very challenging, as it demands ultrafine tuning of the antenna length. Alternatively, in the following we demonstrate that by loading monoalyer graphene under the metallic antennas, the enhancement effect can be accurately and actively tuned as needed. We also employ this active device to detect weak vibrational fingerprints of monolayer protein, which can hardly be resolved unless there is sufficient overlap between the plasmonic resonance and the fingerprints bands. Our active metasurface devices consist of nanorod antennas with length L = 1.64 μm and gap width g = 30 nm (Figure 4a,b, Supporting Information, IX) and a substrate of 285 nm SiO_2 grown on a Pt mirror. A layer of graphene is sandwiched between the antennas and the substrate, and a gate voltage, V_g, is applied between the Pt mirror and the graphene layer to change the graphene Fermi level and, thus, its optical conductivity. The metasurface plasmon−phonon resonance blue-shifts as the graphene optical conductivity increases (Figure 4c).[29] Full-wave simulations show that in these active devices graphene surface plasmon is excited and confined to the surface of graphene inside the antenna gaps, resulting in strong light intensity enhancement (Figure 4e, Supporting Information, X) and larger light−protein interaction area compared to passive devices without graphene (Figure 2e,

DOI: 10.1021/acsphotonics.8b01470
ACS Photonics 2019, 6, 501−509

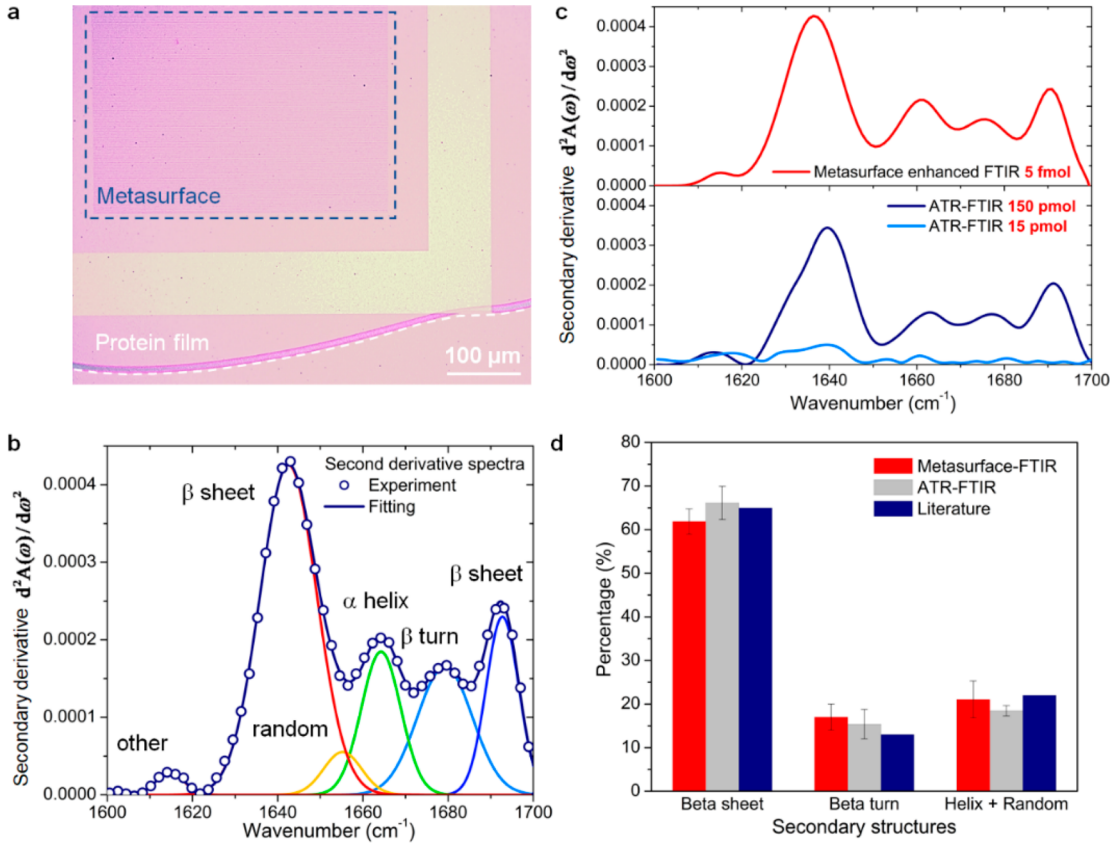

Figure 5. Secondary structures of the monolayer IgG. (a) An optical image showing a uniform layer of antibody IgG (as indicated by white dashed line) formed on metasurface sensor by physisorption. Part of the metasurface sensor is as shown inside the blue dashed line. (b) Fitting of the second derivative spectrum, $d^2A(\omega)/d\omega^2$, derived from the absorptance spectrum, $A(\omega)$, of the Amide I band of the human antibody IgG measured using a passive metasurface sensor. (c) Top panel: the corrected second derivative spectrum of the Amide I band obtained by using the metasurface sensor incubated with 5 fmol IgG. Bottom panel: the second derivative spectra of IgG obtained by using conventional ATR-FTIR measurements and 150 pmol of IgG. (d) Determination of the percentage of the secondary structures of the human IgG protein using metasurface-enhanced FTIR and ATR-FTIR.

Supporting Information, IV). What is more, the addition of graphene barely affects the quality factor of optical resonance (Supporting Information, XVI).[35] Compared to the devices that only use graphene as the functional material, our active device can provide both stronger confinement from the metallic antennas and the tunability of the plasmonic resonance, therefore capable of resolving even weaker fingerprints.

A protein A/G monolayer immobilized onto the device surfaces was used to characterize our active metasurface sensors. At $V_g = -10$ V, the metasurface resonance located at $\omega = 1427$ cm^{-1} and was more than 100 cm^{-1} away from the amide bands. In this case, the Amide I band around $\omega_I = 1640$ cm^{-1} was very weak, and the Amide II around $\omega_{II} = 1533$ cm^{-1} was almost undetectable (Figure 4c). As the gate voltage was increased to 80 V, the metasurface resonance blue-shifted to 1512 cm^{-1}, nicely overlapping the Amide II band. In contrast to the weak signals of fingerprints at $V_g = -10$ V, at $V_g = 80$ V, the measured spectrum showed very pronounced absorption bands at $\omega_I = 1640$ cm^{-1} and $\omega_{II} = 1533$ cm^{-1} (Figure 4c). Moreover, a fingerprint located around $\omega = 1460$ cm^{-1} corresponding to CH_2 bending vibrational mode was observable only when it spectrally overlapped with the metasurface resonance at $V_g = -10$ to 30 V, and became unresolvable as V_g increases to 40 V and beyond (Supporting Information, XI). In this way, we demonstrated effective enhancement of the weak spectral signals by accurately tuning the plasmonic resonance frequency and thus weak fingerprint signals can be differentiated from device background noise. Accordingly, the peak value of relative absorptance, $|\Delta R/R|$, increased from 5.47% to 12.84% for the Amide I band and from 4.82% to 13.82% for the Amide II band (Figure 4d), both in good agreement with full-wave simulations. As the graphene doping was increased from 1.5×10^{12} to 4×10^{12} cm^{-2}, the simulated relative absorptance peak value increased from 9.16% to 19.1% for the Amide I band and from 9.26% to 20.0% for the Amide II band (Supporting Information, XII). At the same time, the difference between the metasurface resonance and the Amide I band, $\Delta\omega = |\omega_{meta} - \omega_{amideI}|$, decreased from 212 to 122 cm^{-1}. For Amide II band, the difference,$\Delta\omega = |\omega_{meta} - \omega_{amideII}|$, decreased from 105 to 15 cm^{-1} (Figure 4f). In comparison, spectra measured from a protein A/G monolayer immobilized on a SiO_2/Au substrate showed no features of the amide bands (spectrum labeled as "SiO_2−Au" in Figure 4d and details in Supporting Information, XIII). By using active tuning, the metasurface resonance can be precisely controlled at ∼0.95 cm^{-1}/V, which, in combination with nanofabrication that defines antenna length and thus the initial spectral location of the metasurface resonance, offers a unique way to maximize the fingerprinting capabilities of metasurface sensors.

DOI: 10.1021/acsphotonics.8b01470
ACS Photonics 2019, 6, 501−509

Beyond the ability to fingerprinting protein molecules through their characteristic mid-IR vibrational modes, another important application of mid-IR spectroscopy is to determine the secondary structure of proteins. This is typically done by quantitative analyses of the Amide I band, which is sensitively dependent on the 3D configuration of the protein backbone.[36] Specifically, the formation of hydrogen bonds between the amine hydrogen and carbonyl oxygen atoms in the peptide backbone of protein secondary structures, such as α-helices, β-sheets, and β-turns, leads to subtle but characteristic modifications to the Amide I band.[37−39] By taking the second derivative of the Amide I band, such subtle features can be resolved and thus the protein secondary structure can be inferred. Large quantities of proteins are usually needed for obtaining mid-IR spectra with a sufficiently high signal-to-noise ratio, which is a prerequisite for reliable second derivative spectra. By taking advantage of the strong interactions between light and biomolecules in our metasurface sensors, we can determine protein secondary structures with substantially increased sensitivity.

We immobilized antibody IgG molecules onto our metasurface sensors by physisorption and obtained the absorptance spectra of the Amide I band (Figure 5a). We took the second derivative of the absorptance spectra and decomposed the result into a set of Gaussian peaks (Figure 5b). Using the location of these Gaussian peaks as a reference, we decomposed the absorptance spectra of the Amide I band into a set of constituent components (Figure S14(a)), each representing the C═O vibrational mode influenced by a specific 3D protein backbone configuration (e.g., α-helix, β-sheet, β-turn). The strong coupling between protein molecules and the metasurface sensor causes blue-shifts of the amide bands (Figure 2d). We conducted simulations to quantify such blue-shifts (Figure S14(b)) and corrected the raw second derivative spectra by red-shifting the constituent Gaussian peaks (Figure S14(c)). This correction is crucial for assigning peaks in the second derivative spectra to specific protein secondary structures.

We compared second derivative spectra taken by our metasurface sensors with those taken by attenuated total reflection (ATR) FTIR, which is a commonly used analytical tool for spectroscopic study of proteins (Figure 5c). The comparison shows that the spectrum obtained using our biosensor and ∼5 fmol of IgG is in good agreement with that obtained using ATR-FTIR and ∼150 pmol of IgG, in terms of the position and magnitude of the constituent peaks. The second derivative spectrum taken by ATR-FTIR became too noisy to reveal any meaningful information when the amount of protein molecules was decreased to ∼15 pmol. This comparative study indicates that the sensitivity of determining protein secondary structures using the metasurface devices is enhanced by more than 4 orders of magnitude compare to standard ATR-FTIR. Analyses of the second derivative spectra reveal that the human protein IgG we used is composed of 61.9% β-turns, 21.1% β-sheets, and a combination of 17.0% α-helixes and random structures. The results are in good agreement with the measurements using ATR-FTIR as well as those reported in the literature (Figure 5d).[11]

Metasurfaces provide a unique platform for label-free sensing of biomolecules via surface enhanced infrared spectroscopy with high sensitivity and specificity. In this platform, the interaction between infrared light and biomolecules is greatly enhanced because protein molecules and surface plasmon fields are colocated in the small gaps of nanoantennas. Reduced radiation losses due to the coupling between the nanoantennas and the back mirror, and coupling between the plasmonic resonance of the nanoantennas and SiO_2 phonon resonance lead to a metasurface resonance with a Q-factor of ∼10, which enables the detection of protein IgG molecules with concentrations as low as 30 pM. The combination of passive tuning by changing the nanoantenna geometrics and active tuning by adjusting bias voltages applied to the metasurface sensors is utilized to acurrately overlap the metasurface resonance with biomolecules' vibrational modes. This enables the detection of mid-IR fingerprints of monolayer protein A/G molecules. Enhanced fingerprinting capabilities is accompanied by spectral shifts of the fingerprints. The dependence of such spectral shifts on the detuning of the fingerprints from the metasurface resonance was observed in experiments and quantified in simulations. Based on this, we were able to conduct accurate analyses of the protein Amide I band, which contains the conformational information on the protein backbone, and determined the secondary structure of protein IgG. The results show a good agreement with conventional ATR-FTIR measurements with an improvement of sensitivity by more than 4 orders of magnitude.

The high-performance multifunctional metasurface-based optical platform demonstrated in this work is desirable for biosensing applications including healthcare monitoring and disease diagnosis. For instance, determining the concentration level of biomolecules such as insulin and glucose is very critical in diabetes screening and therapy. Many human disorder, such as Alzheimer's and type II diabetes, are accompanied by the structural change and misfolding of related protein molecules. Analyzing the secondary structure of pathological proteins can help better understand mechanisms causing the diseases. In addition, our devices may also help provide insight into higher order structures of proteins, such as the tertiary structures of Amide II and Amide II′ bands.[40]

METHODS

Detection of IgG Concentration in Passive Metasurface Sensors. A monolayer of protein A/G as binding sites of IgG was incubated on the surface of a metasurface sensor by physisorption. The sensor was then incubated in a series of IgG antibody solutions at increasing concentrations, which resulted in increasing surface coverage of the devices by monolayer IgG. Mid-IR spectroscopic measurements were conducted at the end of each IgG incubation to observe the resonant wavelength shifts of the metasurface resonance and the spectral fingerprints of the amide bands. The resonant wavelength shift $\Delta\lambda$ is proportional to the perturbation of local optical refractive index Δn, which scales with surface coverage of IgG antibody molecules, and can be well described by the Langmuir adsorption isotherm model:[19,32]

$$\Delta\lambda = \frac{\Delta\lambda_{max}[C]}{K_d + [C]}$$

where $\Delta\lambda_{max}$ is the saturated wavelength shift, corresponding to complete surface coverage by an IgG monolayer, $[C]$ is the concentration of IgG, and K_d is the Langmuir equilibrium constant of dissociation. The latter is the ratio of desorption rate K_{off} and adsorption rate K_{on} and characterizes the binding strength (e.g., a low K_d indicates strong binding affinity, where adsorption overwhelms desorption at equilibrium).

DOI: 10.1021/acsphotonics.8b01470
ACS Photonics 2019, 6, 501−509

Enhancing Biomolecule Fingerprinting by Adjusting Antenna Geometry. The metasurface resonance was blue-shifted by decreasing the length of nanoantennas from $L = 2.44$ to 1.54 μm in several metasurface sensors. For each sensor, a monolayer of protein A/G was immobilized on the device surface. A monolayer of IgG was then formed by incubating the device in 3 μM IgG solutions until equilibrium (i.e., nearly complete formation of an IgG monolayer), followed by rinsing the device in DI water to remove unbound residues.

Coupled Oscillator Model. Four oscillators are considered in our model: the plasmonic resonance of gold nanoantennas, the phonon resonance of the SiO_2 spacer, and Amide I/II vibrational modes. Plasmonic nanoantennas can directly interact with the incident light, and localize optical energy into antenna gaps; therefore, plasmonic resonance is a "bright" mode. The other three modes can only weakly interact with incident light; therefore, they are "dark" modes. Under the assumption that the coupling between the nanoantenna plasmonic mode and SiO_2 phonon mode is much stronger than the coupling between the plasmonic mode and amide vibrational modes, we can derive the analytical solution of the susceptibility of the amide oscillators:

$$\chi_{\mathrm{amideI(II)}}(\omega) \approx -\frac{1}{-\omega^2 + \omega_{\mathrm{amideI(II)}}^2 + i\omega\gamma_{\mathrm{amideI(II)}}} \times \frac{K_{\text{meta-amide}}}{\left(-\omega^2 + \omega_{\mathrm{plasmon}}^2 + i\omega\gamma_{\mathrm{plasmon}} - \frac{K_{\mathrm{plasmon-phonon}}^2}{-\omega^2 + \omega_{\mathrm{SiO_2}}^2 + i\omega\gamma_{\mathrm{SiO_2}}}\right)}$$

where $\omega_{\text{amide I(II)}}$, ω_{plasmon}, and ω_{SiO2} are the resonant frequencies of the amide vibrational modes, nanoantenna plasmonic mode, and SiO_2 phonon mode, respectively; $\gamma_{\text{amide I(II)}}$, γ_{plasmon}, and γ_{SiO2} are the damping rates of the three types of oscillators, respectively; $\kappa_{\text{plasmon-phonon}}$ is the coupling coefficient between the plasmonic mode and SiO_2 phonon mode; $\kappa_{\text{meta-amide}}$ is the coupling coefficient between the plasmon-phonon mode of the metasurface and the amide modes. This model predicts that the oscillation strength of the amide modes, represented by $\chi_{\text{amide I(II)}}$, depends on the spectral separation between the amide modes (first term of the equation) and the metasurface plasmon−phonon mode (second term of the equation), as well as the coupling coefficient between the two, $\kappa_{\text{meta-amide}}$. The details of the coupled oscillator model can be found in the section VIII of the Supporting Information.

■ ASSOCIATED CONTENT

Supporting Information

The Supporting Information is available free of charge on the ACS Publications website at DOI: 10.1021/acsphotonics.8b01470.

Detailed procedure of the device fabrication and the protein immobilization protocol. Charaterization of single-layer graphene. Additional full-wave simulations for passive as well as active biosensing devices. Detailed description of coupled oscillator model and fitting results. Addtional SEM and optical microscopic images of active metasurface devices. Zoom-in reflectance spectra of active tuning device as a function of gating voltage. Analysis procedure of secondary structure of monolayer antibody IgG (PDF).

■ AUTHOR INFORMATION

Corresponding Authors

*E-mail: zl2275@columbia.edu.
*E-mail: qlin@columbia.edu.
*E-mail: ny2214@columbia.edu.

ORCID

Zhaoyi Li: 0000-0003-3661-8438
Yibo Zhu: 0000-0003-4323-1290

Author Contributions

†These authors contributed equally to this work.

Notes

The authors declare no competing financial interest.

■ ACKNOWLEDGMENTS

The work was supported by a Defense Advanced Research Projects Agency Young Faculty Award (Grant No. D15AP00111), the Air Force Office of Scientific Research (Grant Nos. FA9550-14-1-0389 and FA9550-16-1-0322), and the National Science Foundation (Grant No. ECCS-1307948). Research was carried out in part at the Center for Functional Nanomaterials, Brookhaven National Laboratory, which is supported by the U.S. Department of Energy, Office of Basic Energy Sciences (Contract No. DE-SC0012704).

■ REFERENCES

(1) Lee, H.; Choi, T. K.; Lee, Y. B.; Cho, H. R.; Ghaffari, R.; Wang, L.; Choi, H. J.; Chung, T. D.; Lu, N.; Hyeon, T. A graphene-based electrochemical device with thermoresponsive microneedles for diabetes monitoring and therapy. *Nat. Nanotechnol.* **2016**, *11*, 566.

(2) Gao, W.; Emaminejad, S.; Nyein, H. Y. Y.; Challa, S.; Chen, K.; Peck, A.; Fahad, H. M.; Ota, H.; Shiraki, H.; Kiriya, D. Fully integrated wearable sensor arrays for multiplexed in situ perspiration analysis. *Nature* **2016**, *529*, 509−514.

(3) Zeng, S.; Sreekanth, K. V.; Shang, J.; Yu, T.; Chen, C. K.; Yin, F.; Baillargeat, D.; Coquet, P.; Ho, H. P.; Kabashin, A. V.; Yong, K. T. Graphene-Gold Metasurface Architectures for Ultrasensitive Plasmonic Biosensing. *Adv. Mater.* **2015**, *27*, 6163−9.

(4) Cui, Y.; Wei, Q.; Park, H.; Lieber, C. M. Nanowire nanosensors for highly sensitive and selective detection of biological and chemical species. *Science* **2001**, *293*, 1289−1292.

(5) Gao, N.; Gao, T.; Yang, X.; Dai, X.; Zhou, W.; Zhang, A.; Lieber, C. M. Specific detection of biomolecules in physiological solutions using graphene transistor biosensors. *Proc. Natl. Acad. Sci. U. S. A.* **2016**, *113*, 14633−14638.

(6) Kneipp, K.; Wang, Y.; Kneipp, H.; Perelman, L. T.; Itzkan, I.; Dasari, R. R.; Feld, M. S. Single molecule detection using surface-enhanced Raman scattering (SERS). *Phys. Rev. Lett.* **1997**, *78*, 1667.

(7) Cao, Y. C.; Jin, R.; Mirkin, C. A. Nanoparticles with Raman spectroscopic fingerprints for DNA and RNA detection. *Science* **2002**, *297*, 1536−1540.

(8) Boutet, S.; Lomb, L.; Williams, G. J.; Barends, T. R.; Aquila, A.; Doak, R. B.; Weierstall, U.; DePonte, D. P.; Steinbrener, J.; Shoeman, R. L.; et al. High-resolution protein structure determination by serial femtosecond crystallography. *Science* **2012**, *337*, 362−364.

(9) Wuthrich, K. Protein structure determination in solution by nuclear magnetic resonance spectroscopy. *Science* **1989**, *243*, 45.

(10) Greenfield, N. J. Using circular dichroism spectra to estimate protein secondary structure. *Nature protocols* **2007**, *1*, 2876.

(11) Yang, H.; Yang, S.; Kong, J.; Dong, A.; Yu, S. Obtaining information about protein secondary structures in aqueous solution using Fourier transform IR spectroscopy. *Nat. Protoc.* **2015**, *10*, 382.

(12) Wu, C.; Khanikaev, A. B.; Adato, R.; Arju, N.; Yanik, A. A.; Altug, H.; Shvets, G. Fano-resonant asymmetric metamaterials for ultrasensitive spectroscopy and identification of molecular monolayers. *Nat. Mater.* **2012**, *11*, 69−75.

DOI: 10.1021/acsphotonics.8b01470
ACS Photonics 2019, 6, 501−509

(13) Adato, R.; Yanik, A. A.; Amsden, J. J.; Kaplan, D. L.; Omenetto, F. G.; Hong, M. K.; Erramilli, S.; Altug, H. Ultra-sensitive vibrational spectroscopy of protein monolayers with plasmonic nanoantenna arrays. *Proc. Natl. Acad. Sci. U. S. A.* **2009**, *106*, 19227−19232.
(14) Yang, J.; Palla, M.; Bosco, F. G.; Rindzevicius, T.; Alstrøm, T. S.; Schmidt, M. S.; Boisen, A.; Ju, J.; Lin, Q. Surface-enhanced Raman spectroscopy based quantitative bioassay on aptamer-functionalized nanopillars using large-area Raman mapping. *ACS Nano* **2013**, *7*, 5350−5359.
(15) Cao, C.; Zhang, J.; Wen, X.; Dodson, S. L.; Dao, N. T.; Wong, L. M.; Wang, S.; Li, S.; Phan, A. T. a.; Xiong, Q. Metamaterials-based label-free nanosensor for conformation and affinity biosensing. *ACS Nano* **2013**, *7*, 7583−7591.
(16) Yanik, A. A.; Cetin, A. E.; Huang, M.; Artar, A.; Mousavi, S. H.; Khanikaev, A.; Connor, J. H.; Shvets, G.; Altug, H. Seeing protein monolayers with naked eye through plasmonic Fano resonances. *Proc. Natl. Acad. Sci. U. S. A.* **2011**, *108*, 11784−11789.
(17) Cetin, A. E.; Altug, H. Fano resonant ring/disk plasmonic nanocavities on conducting substrates for advanced biosensing. *ACS Nano* **2012**, *6*, 9989−9995.
(18) Sreekanth, K. V.; Alapan, Y.; ElKabbash, M.; Ilker, E.; Hinczewski, M.; Gurkan, U. A.; De Luca, A.; Strangi, G. Extreme sensitivity biosensing platform based on hyperbolic metamaterials. *Nat. Mater.* **2016**, *15*, 621.
(19) Guo, Q.; Zhu, H.; Liu, F.; Zhu, A. Y.; Reed, J. C.; Yi, F.; Cubukcu, E. Silicon-on-glass graphene-functionalized leaky cavity mode nanophotonic biosensor. *ACS Photonics* **2014**, *1*, 221−227.
(20) Rodrigo, D.; Limaj, O.; Janner, D.; Etezadi, D.; de Abajo, F. J. G.; Pruneri, V.; Altug, H. Mid-infrared plasmonic biosensing with graphene. *Science* **2015**, *349*, 165−168.
(21) Hu, H.; Yang, X.; Zhai, F.; Hu, D.; Liu, R.; Liu, K.; Sun, Z.; Dai, Q. Far-field nanoscale infrared spectroscopy of vibrational fingerprints of molecules with graphene plasmons. *Nat. Commun.* **2016**, *7*, 12334.
(22) Yu, N.; Capasso, F. Flat optics with designer metasurfaces. *Nat. Mater.* **2014**, *13*, 139.
(23) Kildishev, A. V.; Boltasseva, A.; Shalaev, V. M. Planar photonics with metasurfaces. *Science* **2013**, *339*, 1232009.
(24) Chen, H.-T.; Taylor, A. J.; Yu, N. A review of metasurfaces: physics and applications. *Rep. Prog. Phys.* **2016**, *79*, No. 076401.
(25) Adato, R.; Altug, H. In-situ ultra-sensitive infrared absorption spectroscopy of biomolecule interactions in real time with plasmonic nanoantennas. *Nat. Commun.* **2013**, *4*, 2154.
(26) Cetin, A. E.; Etezadi, D.; Galarreta, B. C.; Busson, M. P.; Eksioglu, Y.; Altug, H. Plasmonic nanohole arrays on a robust hybrid substrate for highly sensitive label-free biosensing. *ACS Photonics* **2015**, *2*, 1167−1174.
(27) De Abajo, F. G. Colloquium: Light scattering by particle and hole arrays. *Rev. Mod. Phys.* **2007**, *79*, 1267.
(28) Schuller, J. A.; Barnard, E. S.; Cai, W.; Jun, Y. C.; White, J. S.; Brongersma, M. L. Plasmonics for extreme light concentration and manipulation. *Nat. Mater.* **2010**, *9*, 193−204.
(29) Li, Z.; Yu, N. Modulation of mid-infrared light using graphene-metal plasmonic antennas. *Appl. Phys. Lett.* **2013**, *102*, 131108.
(30) Seok, T. J.; Jamshidi, A.; Kim, M.; Dhuey, S.; Lakhani, A.; Choo, H.; Schuck, P. J.; Cabrini, S.; Schwartzberg, A. M.; Bokor, J. Radiation engineering of optical antennas for maximum field enhancement. *Nano Lett.* **2011**, *11*, 2606−2610.
(31) Zhu, A. Y.; Yi, F.; Reed, J. C.; Zhu, H.; Cubukcu, E. Optoelectromechanical multimodal biosensor with graphene active region. *Nano Lett.* **2014**, *14*, 5641−5649.
(32) Laidler, K. J. *Chemical kinetics*; Prentice Hall, 1987.
(33) Brar, V. W.; Jang, M. S.; Sherrott, M.; Kim, S.; Lopez, J. J.; Kim, L. B.; Choi, M.; Atwater, H. Hybrid surface-phonon-plasmon polariton modes in graphene/monolayer h-BN heterostructures. *Nano Lett.* **2014**, *14*, 3876−3880.
(34) Memmi, H.; Benson, O.; Sadofev, S.; Kalusniak, S. Strong coupling between surface plasmon polaritons and molecular vibrations. *Phys. Rev. Lett.* **2017**, *118*, 126802.
(35) Zhu, Y.; Li, Z.; Hao, Z.; DiMarco, C.; Maturavongsadit, P.; Hao, Y.; Lu, M.; Stein, A.; Wang, Q.; Hone, J. Optical conductivity-based ultrasensitive mid-infrared biosensing on a hybrid metasurface. *Light: Sci. Appl.* **2018**, *7*, 67.
(36) Barth, A. Infrared spectroscopy of proteins. *Biochim. Biophys. Acta, Bioenerg.* **2007**, *1767*, 1073−1101.
(37) Etezadi, D.; Warner, I.; Blaine, J.; Ruggeri, F. S.; Dietler, G.; Lashuel, H.; Altug, H. Nanoplasmonic mid-infrared biosensor for in vitro protein secondary structure detection. *Light: Sci. Appl.* **2017**, *6*, 17029.
(38) Arrondo, J. L. R.; Muga, A.; Castresana, J.; Goñi, F. M. Quantitative studies of the structure of proteins in solution by Fourier-transform infrared spectroscopy. *Prog. Biophys. Mol. Biol.* **1993**, *59*, 23−56.
(39) Kong, J.; Yu, S. Fourier transform infrared spectroscopic analysis of protein secondary structures. *Acta Biochim. Biophys. Sin.* **2007**, *39*, 549−559.
(40) Smith, J. R.; Cicerone, M. T.; Meuse, C. W. Tertiary structure changes in albumin upon surface adsorption observed via fourier transform infrared spectroscopy. *Langmuir* **2009**, *25*, 4571−4578.

DOI: 10.1021/acsphotonics.8b01470
ACS Photonics 2019, 6, 501−509